

## A MODEL FOR THE NUMERICAL SIMULATION OF RIVULET EVOLUTION ON A CIRCULAR CYLINDER IN AN AIR FLOW

A.C. Robertson, I.J. Taylor

*Department of Mechanical Engineering, University of Strathclyde, Glasgow, UK, G1 1XJ*

S.K. Wilson, B.R. Duffy and J.M. Sullivan

*Department of Mathematics, University of Strathclyde, Glasgow, UK, G1 1XH*

### ABSTRACT

*The simultaneous occurrence of rain and wind can generate rivulets of water on the cables of cable-stayed bridges. Under certain conditions the interaction of these rivulets with the local aerodynamic field may result in Rain Wind Induced Vibration (RWIV). A method to model this phenomenon computationally is currently under development at the University of Strathclyde. The current paper presents a two-dimensional model for the evolution of a thin film of water on the outer surface of a circular cylinder subject to pressure, shear, surface-tension and gravitational forces. Numerical simulations of the resulting evolution equation using a bespoke pseudo-spectral solver capture the formation of ‘rivulets’; the geometry, location and growth rate of which are all in good agreement with previous studies.*

### 1. INTRODUCTION

The presence of rivulets of rain-water on the cables of cable-stayed bridges which are subject to an external aerodynamic field (wind) can result in a large amplitude, low frequency, dynamic instability known as Rain Wind Induced Vibration (RWIV). In contrast to other aeroelastic instabilities these are present only over a restricted range of wind velocities and only for cables that descend in the direction of the wind. Although not fully understood, RWIV is thought to be associated with rivulets forming near the separation points of the external flow, and thus only with the correspondingly limited conditions under which this occurs. As such it is generally accepted that these rivulets must be present for this vibration to occur. Therefore any numerical simulation of the RWIV instability should also include the evolution, and perhaps the formation, of these rivulets.

Since the first work by Hikami and Shiraishi

(1988), RWIV studies have primarily consisted of either full scale ‘in-situ’ investigations (Zuo et al., 2008), wind tunnel tests (Matsumoto et al., 2007) or analytical modelling (Peil and Dreyer, 2007). To complement these a method for modelling this phenomenon computationally is currently under development by the authors at the University of Strathclyde.

Preceding work by Robertson and Taylor (2007) investigating both static and oscillating artificial rivulets has identified key features of the driving mechanism of RWIV. The research presented herein represents the next stage of this investigation, and uses the lubrication approximation to develop a two-dimensional model that simulates the interaction between the external aerodynamic field (the wind), and a thin film of rain-water on a horizontal circular cylinder. An evolution equation for this film subject to the normal and tangential stress due to the wind in addition to the forces of surface tension and gravity is derived. A bespoke pseudo-spectral solver for this equation is developed and verified, and results for a number of combinations of loading are presented.

### 2. MODEL

Two-dimensional, unsteady flow of a thin film of incompressible viscous fluid with uniform dynamic viscosity  $\mu$  and density  $\rho$  on the outer surface of a stationary horizontal circular cylinder of radius  $R$  is considered. The outer free surface of this film is subject to a prescribed normal stress (‘pressure’),  $P = P(\theta, t)$ , and prescribed tangential stress (‘shear’),  $T = T(\theta, t)$ , exerted by the external aerodynamic field on the free surface of the film (figure 1).

#### 2.1. Model Description

We take the film to be thin, its aspect ratio  $\epsilon$  (defined by  $\epsilon = H/R$ , where  $H$  denotes a typical

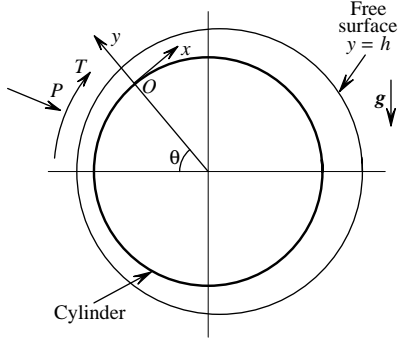


Figure 1: A thin fluid film on a cylinder.

film thickness) satisfying  $\epsilon \ll 1$ .

Initially we refer the description to polar coordinates  $r, \theta, z$  with the  $z$  axis along the axis of the cylinder and with  $\theta$  ( $-\pi < \theta \leq \pi$ ) measured from the horizontal on the upstream (left-hand) side of the cylinder; then the surface of the cylinder is given by  $r = R$ . We denote film thickness by  $h = h(\theta, t)$  (unknown *a priori*); then the free surface of the film is given by  $r = R + h$ . Near any station  $\theta = \text{constant}$  we may alternatively refer the description to a local Cartesian coordinate system  $Oxyz$  with  $Ox$  tangential to the cylinder (increasing in the direction of increasing  $\theta$ , so that  $x = R\theta + \text{constant}$ ) and  $Oy$  along the outward normal to the cylinder, with  $y$  defined by  $y = r - R$ , so that the cylinder is at  $y = 0$  and the free surface is at  $y = h$ . In the latter coordinate system the governing mass-conservation and Navier–Stokes equations give, at leading order in  $\epsilon$ ,

$$u_x + v_y = 0, \quad (1)$$

$$0 = -p_x - \rho g \cos \theta + \mu u_{yy}, \quad (2)$$

$$0 = -p_y, \quad (3)$$

where we have written

$$\mathbf{u} = u\mathbf{i} + v\mathbf{j}, \quad (4)$$

and

$$\mathbf{g} = -g(\mathbf{i} \cos \theta + \mathbf{j} \sin \theta). \quad (5)$$

Equations (1)–(3) are subject to the no-slip and no-penetration conditions on the cylinder:

$$u = v = 0 \quad \text{on} \quad y = 0, \quad (6)$$

and, at the free surface to the kinematic condition

$$v = h_t + uh_x \quad \text{on} \quad y = h, \quad (7)$$

the tangential stress condition

$$\mu u_y = T \quad \text{on} \quad y = h, \quad (8)$$

and the normal stress condition

$$p = \gamma \kappa + P \quad \text{on} \quad y = h, \quad (9)$$

where  $\gamma$  is the coefficient of surface tension,  $\kappa$  is the mean curvature of the free surface, given to first order by

$$\kappa = \frac{1}{R} - \frac{1}{R^2}(h + h_{\theta\theta}). \quad (10)$$

The azimuthal volume flux of fluid in the film is given by

$$Q = \int_0^h u \, dy, \quad (11)$$

and using this and (1) we may replace (7) by the conservation law

$$h_t + Q_x = 0. \quad (12)$$

## 2.2. Evolution Equation for $h(\theta, t)$

Integrating (3) subject to (9) we obtain

$$p = \gamma \kappa + P \quad (13)$$

(independent of  $y$ ), and then integrating (2) with respect to  $y$  subject to (6) and (8) we obtain

$$u = -\frac{1}{2\mu}(\rho g \cos \theta + p_x)(2hy - y^2) + \frac{T y}{\mu}. \quad (14)$$

Therefore from (11)

$$Q = -\frac{1}{3\mu}(\rho g \cos \theta + p_x)h^3 + \frac{T h^2}{2\mu}. \quad (15)$$

Finally, substituting (15) into (12) and using (10) and (13) leads to the evolution equation for  $h(\theta, t)$ :

$$h_t + \left( \frac{T h^2}{2\mu R} \right)_\theta - \left[ \frac{h^3}{3\mu R} \left( \rho g \cos \theta - \frac{\gamma}{R^3}(h + h_{\theta\theta})_\theta + \frac{P_\theta}{R} \right) \right]_\theta = 0. \quad (16)$$

(which is consistent with the corresponding equation given by Lemaitre et al. (2007) in the case of flow on a static cylinder). This equation is to be solved subject to an initial condition of the form  $h(\theta, 0) = h_0(\theta)$ , where  $h_0(\theta)$  is the initial thickness of the film. For definiteness in the present work we have chosen an initially uniform film  $h_0 = \text{constant}$ , and allow the film to evolve according to (16) to see if ‘rivulets’ develop.

### 3. NUMERICAL SOLVER

The evolution equation (16) for film thickness  $h(\theta, t)$  is a fourth order, non-linear, non-constant coefficient partial differential equation, which cannot, in general, be solved analytically. Therefore, a pseudo-spectral solver using an  $N$  point Fourier spectral mode in space and a fourth order Adams-Bashforth time marching algorithm was constructed. This numerical method was chosen specifically because of the periodic nature of the problem and the required rate of convergence to, and the presumed smoothness of, the final result.

#### 3.1. Parameter Selection

Efficient usage of the Fast Fourier Transform (FFT) requires  $N$  to be a power of 2. Through a computational convergence study, a spatial resolution of  $N = 128$  points was found to provide the optimum ‘trade-off’ between speed, accuracy and stability; a similar study revealed a time-step of  $0.5\mu\text{s}$  to be optimal. Both parameters were therefore fixed at these values throughout the present work.

Standard values for gravity and the properties at an air-water interface at  $25^\circ\text{C}$  were selected; see table 1. Other parameter values were chosen to correspond to a typical Reynolds number for RWIV of  $Re \simeq 1 \times 10^5$ , or to ensure the value of  $h_0/R = 6.3 \times 10^{-3}$  as used by Lemaitre et al. (2007) and Flamand (1995).

Property	Value
Cylinder Radius, $R$	0.08 m
Initial film height, $h_0$	$5 \times 10^{-4}$ m
Gravity, $g$	$9.806 \text{ m/s}^2$
Density, $\rho$	$1000 \text{ kg/m}^3$
Dynamic viscosity, $\mu$	$1.002 \times 10^{-3} \text{ Ns/m}$
Surface tension, $\gamma$	$72 \times 10^{-3} \text{ N/m}$

Table 1: *Values of parameters used.*

The distributions of pressure  $P$  and shear  $T$  due to the aerodynamic field were, in the present work, determined in a static manner based upon the aerodynamic field around a dry cylinder. Experimental values for the mean aerodynamic coefficients  $C_P$  and  $C_F$  at the Reynolds number under investigation here,  $Re = 1 \times 10^5$ , were measured by Achenbach (1968) (figure 2). The pseudo-spectral method however is susceptible to aliasing of high frequencies especially in the non-linear terms present in (16). To avoid this and to maintain the stability of the method (the convergence rate of the pseudo-spectral method is

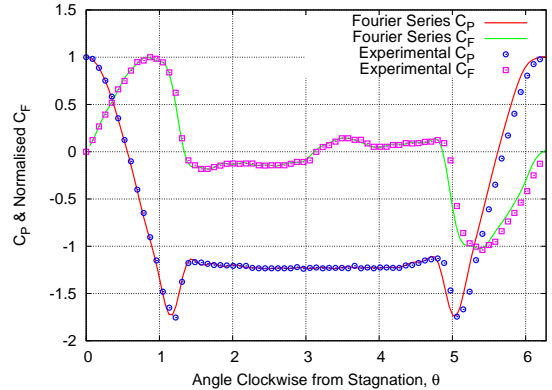


Figure 2: *Comparison of aerodynamic coefficients at  $Re = 1 \times 10^5$  given by Achenbach (1968) and those used in the present study.*

higher for analytic functions), a Fourier series representation of  $C_P$  and  $C_F$  in the form

$$\frac{a_0}{2} + \sum_{n=1}^{20} [a_n \cos(nx) + b_n \sin(nx)] \quad (17)$$

was used; twenty terms of which were found to be sufficient to reproduce the variation of aerodynamic coefficient with angle accurately. A comparison of the truncated series (17) with Achenbach’s original data is shown in figure (2). The series representation of  $C_P$  and  $C_F$  were then appropriately scaled such that the pressure and shear loadings used presently are consistent with those used by Lemaitre et al. (2007) and Flamand (1995).

#### 3.2. Model Verification

Initial verification of the numerical code was achieved through comparison with the work of Reisfeld and Bankoff (1992) who investigated the heating or cooling of a thin viscous film of fluid on a circular cylinder subject to gravity and surface tension. Specific attention was paid to the results of the isothermal case studied, which correspond to the present work when no aerodynamic loading is considered, (i.e. when  $P$  and  $T \equiv 0$ ). Under these conditions the evolution equation (16) represents a competition between the effects of gravity and surface tension on the film. In particular, for the case of large Bond number  $Bo = \rho g R^3 / h_0 \gamma \rightarrow \infty$ , analytical solutions for the evolution can be determined in terms of a reduced time  $\tau = gh_0^2 t / 3\nu R$ , namely

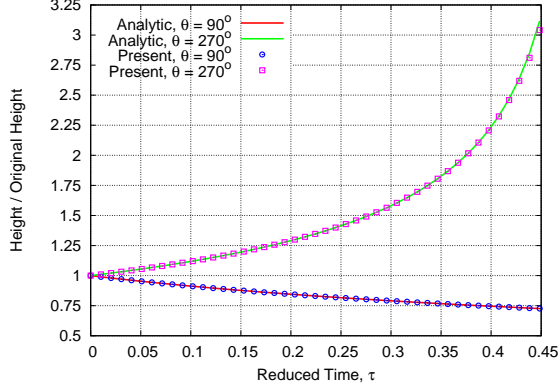


Figure 3: Temporal evolution of present and analytic normalised film height(18 at  $\theta = 90^\circ$  and  $270^\circ$ ).

$$h(\theta, \tau) = \begin{cases} (1 + 2\tau)^{-1/2} & (\theta = \theta_0 = 90^\circ) \\ (1 - 2\tau)^{-1/2} & (\theta = \theta_0 = 270^\circ) \\ (\sin \theta_0 / \sin \theta)^{1/3} & (0^\circ < \theta < 360^\circ, \\ & \theta \neq 180^\circ) \end{cases} \quad (18)$$

In the real case under examination the Bond number,  $Bo = 1.4 \times 10^5$ , is towards the lower end of the physically applicable range for this solution. As such for the purposes of validation the initial height of film,  $h_0$ , and radius of the cylinder,  $R$ , were each increased by a factor of ten to 0.8m and 0.005m respectively, thus maintaining a ratio of  $h_0/R = 6.3 \times 10^{-3}$ , corresponding to a  $Bo = 1.4 \times 10^7$ . This allows a more accurate comparison with the analytical solution. The evolution of normalised film thickness  $h/h_0$  at the upper and lower hemispherical points,  $\theta = 90^\circ$  and  $270^\circ$ , with reduced time  $\tau$  is shown in figure 3. The results show both excellent qualitative and quantitative agreement up to,  $\tau \simeq 0.45$ . For  $0.45 \leq \tau < 0.5$  the numerical calculations become increasingly less accurate as the lubrication approximation begins to break down as the film thickness at  $\theta = 270^\circ$  becomes singular as  $\tau \rightarrow 0.5$ .

#### 4. RESULTS

The relative effects of all four loadings, pressure  $P$ , shear  $T$ , surface tension  $\gamma$  and gravity  $g$  were studied. Four cases of loading combination were considered, namely

- gravity and surface tension ( $T$  and  $P \equiv 0$ ),
- pressure and surface tension ( $T$  and  $g \equiv 0$ ),
- shear and surface tension, ( $P$  and  $g \equiv 0$ ),

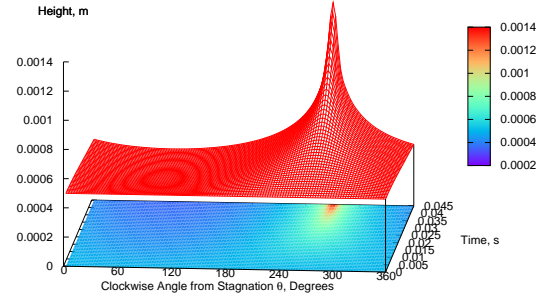


Figure 4: Temporal evolution of film height, under gravity and surface tension effects only.

- full loading ( $P, T, g$  and  $\gamma \neq 0$ ).

#### 4.1. Gravity and Surface Tension Loading

Using the values of  $h_0$  and  $R$  for the real case from table 1, the results show a thinning of the film on the upper surface of the cylinder and a spike growing at  $\theta = 270^\circ$ , figure 4. This fluid accumulation continues to increase until the lubrication approximation is violated and the numerical method is no longer valid. At the equatorial points ( $\theta = 0^\circ$  and  $180^\circ$ ) the film thickness remains approximately constant with time; this is consistent with the analytical solution (18).

The effect of varying the loading due to gravity or surface tension by an order of magnitude from the real values, whilst maintaining  $Bo$  greater than approximately  $1 \times 10^5$ , does not significantly change the solution at the same value of the reduced time,  $\tau$ ; instead this only alters the real time  $t$  taken to arrive at that solution. Indeed if gravity and surface tension are varied such that  $Bo$  remains constant then this temporal variation is minimised. Reducing  $Bo$  significantly below  $1 \times 10^5$ , however, changes the result dramatically, but this is beyond the scope of the present work, and the reader is referred to Reisfeld and Bankoff (1992) for a fuller discussion.

#### 4.2. Pressure and Surface Tension Loading

Under only pressure  $P$  and surface tension  $\gamma$  loading, two symmetric distinct rivulets form, one on the upper and one on the lower surface. Figure 5 shows the evolution of these rivulets which are located just windward of the clockwise and anti-clockwise separation points for a dry cylinder. This is consistent with previous experimental analysis by Bosdogianni and Olivari (1996). Furthermore, the current data com-

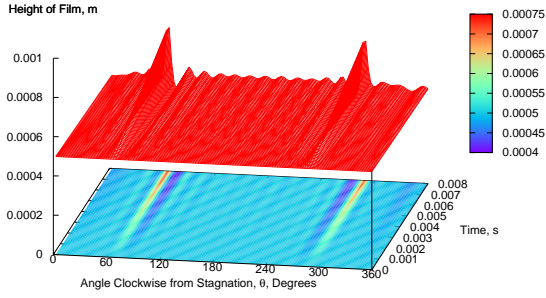


Figure 5: *Temporal evolution of film height, under pressure and surface tension effects only.*

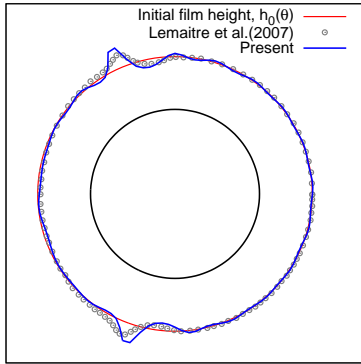


Figure 6: *Comparison of film height ( $100\times$  actual) at  $\tau = 6.9$  ms, with that of Lemaitre et al. (2007), under the effects of pressure and surface tension only.*

compares favourably with the only other computational data available by Lemaitre et al. (2007), as illustrated in figure 6. The discrepancies between the two solutions can be tentatively attributed to the variation in profile used for  $C_P$ .

### 4.3. Shear and Surface Tension Loading

Under only shear  $T$  and surface tension  $\gamma$  loading the results have similarities to those for the previous loading condition (section 4.2). Again symmetric rivulets form just windward of the separation points on both sides of a dry cylinder, figure 7. In this instance, however, the rivulets develop marginally leeward of those in the pressure and surface tension case. It is also noted that the size of the rivulet is approximately the same as that of the previous loading condition. These factors along with similar rates of growth, indicate that the pressure and shear loadings are of

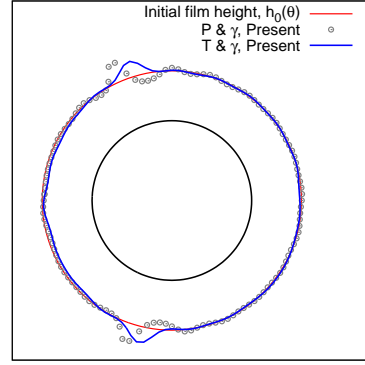


Figure 7: *Comparison of film height ( $100\times$  actual) at  $\tau = 6.9$  ms, under shear and surface tension loading, and under pressure and surface tension loading.*

roughly equal importance. Again these findings are in good agreement with those of Lemaitre et al. (2007) as is a direct comparison between the corresponding cases of shear and surface tension loading, which is omitted for brevity.

### 4.4. Full Loading

Similarly to the previous two cases, under full loading two distinct rivulets form. However, in this case the symmetry of the previous solutions is lost due to the effect of gravity, figures 8 and 9. The rivulets that evolve in this case are thicker on the lower surface and thinner on the upper surface than in previous cases as would be expected. Furthermore, while the point of maximum thickness of the lower rivulet moves leeward from that found under only pressure and surface tension loading (section 4.2), the thinner upper rivulet moves windward, figure 8. This simple result agrees with intuitive expectations and in so doing increases confidence in both model consistency and accuracy. Similarly a final comparison with the work of Lemaitre et al. (2007) shown in figure 9, also shows excellent agreement. This qualitative and quantitative agreement between the present results and those reported in the previous literature mean that the pseudo-spectral solver that has been developed can now confidently be utilised for more in-depth studies and future coupled unsteady simulations.

## 5. CONCLUSION

A numerical model for the evolution of a thin film on the outer surface of a circular cylinder un-

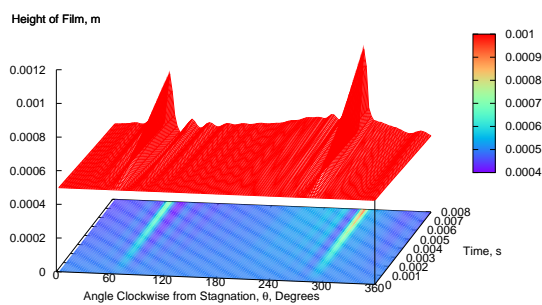


Figure 8: Evolution of film height over time, under full loading conditions.

der the combined effects of pressure, shear, surface tension and gravity has been presented. The pseudo-spectral solver developed to solve the governing evolution equation numerically has been demonstrated to be both self-consistent and to compare well with previous literature under a variety of loading combinations.

Where anticipated two symmetric rivulets form just windward of the separation points of a dry cylinder, while under full loading conditions these rivulets are asymmetric due to the effect of gravity. Likewise, it was found that the relative effects of pressure and shear loading in the cases studied, are roughly comparable, again in excellent agreement with previous work. This verification with respect to the current state of the art allows ongoing developments of the model to be made with an increased degree of confidence.

## 6. ACKNOWLEDGEMENTS

Two of the authors (ACR and JMS) gratefully acknowledge the support of the UK Engineering and Physical Sciences Research Council via Doctoral Training Account studentships.

## 7. REFERENCES

- Achenbach, E., 1968, Distribution of local pressure and skin friction around a circular cylinder in a cross flow up to  $Re = 5 \times 10^6$ . *J. Fluid Mech.* **34**: 625–639.
- Bosdogianni, A., and Olivari, D., 1996, Wind and rain induced oscillations of cables of stayed bridges. *J. Wind Eng. Ind. Aerodyn.* **64**: 171–185.

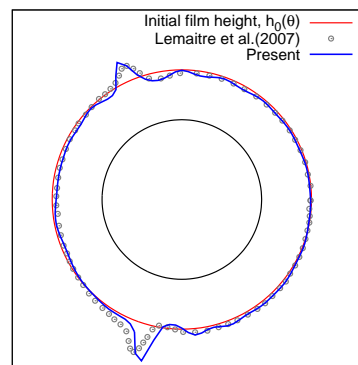


Figure 9: Comparison of film height ( $100 \times$  actual) at  $\tau = 6.9$  ms, with that of Lemaitre et al. (2007), under full loading conditions.

Flamand, O., 1995, Rain-wind induced vibration of cables. *J. Wind Eng. Ind. Aerodyn.* **57**: 353–362.

Hikami, Y., and Shiraishi, N., 1988, Rain-wind induced vibration of cables in cable stayed bridges. *J. Wind Eng. Ind. Aerodyn.* **29**: 409–418.

Lemaitre, C. et al., 2003, Thin water film around a cable subject to wind. *J. Wind Eng. Ind. Aerodyn.* **95**: 1259–1271.

Matsumoto, M. et al., 2007, Karman vortex effects on aerodynamic instabilities of inclined stay cables. In *Proceedings of ICWE12*, 175–182. Cairns: Australia.

Peil, U. and Dreyer, O., 2007, Rain-wind induced vibrations of cables in laminar and turbulent flow. *Wind Struct.* **10**: 83–97. Cairns: Australia.

Reisfeld, B. and Bankoff, S.G., 1992, Non-isothermal flow of a liquid film on a horizontal cylinder. *J. Fluid Mech.* **236**: 167–196.

Robertson, A.C. and Taylor, I.J., 2007, Effect of rivulets on a circular cylinder using a 2D Discrete Vortex Method. In *Proceedings of ICWE12*, 863–870. Cairns: Australia.

Zuo, D., et al., 2008, Field observation of vortex- and rain-wind-induced stay-cable vibrations in a three-dimensional environment. *J. Wind Eng. Ind. Aerodyn.* In press, doi:10.1016/j.jweia.2007.06.046